

Signature and Log-signature for the Study of Empirical Distributions Generated with GANs

J. de Curtò y DíAz¹[0000-0002-8334-4719],
I. de Zarzà i Cubero¹[0000-0002-5844-7871]
, and Hong Yan^{1,2}[0000-0001-9661-3095]

¹ Centre for Intelligent Multidimensional Data Analysis,
HK Science Park, Shatin, Hong Kong

² Department of Electrical Engineering, City University of Hong Kong,
Kowloon, Hong Kong
{decurtoydiaz,dezarzaycubero}@innocimda.com
h.yan@cityu.edu.hk

Abstract. In this paper, we develop a new and systematic method to explore and analyze samples taken by NASA Perseverance on the surface of the planet Mars. A novel in this context PCA adaptive t-SNE is proposed, as well as the introduction of statistical measures to study the goodness of fit of the sample distribution. We go beyond visualization by generating synthetic imagery using Stylegan2-ADA that resemble the original terrain distribution. We also conduct synthetic image generation using the recently introduced Score-based Generative Modeling. We bring forward the use of the recently developed Signature Transform as a way to measure the similarity between image distributions and provide detailed acquaintance and extensive evaluations. We are the first to pioneer RMSE and MAE Signature and log-signature as an alternative to measure GAN convergence. Insights on state-of-the-art instance segmentation of the samples by the use of a model DeepLabv3 are also given.

Keywords: GAN, PCA, t-SNE, Clustering, NASA, Perseverance, Signature Transform, Mars, Segmentation

1 Introduction

Space Exploration has become ubiquitous, from NASA missions to other planets to the privatization of the space sector led by companies such as SpaceX, Blue Origin or Virgin Galactic. The need to study and analyze the amount of data that will be generated in such missions will become essential to improve the Return on Investment. Moreover, the current thread of sending small unmanned autonomous vehicles (nanorovers) to the Moon (e.g. Astrobotic) and in the future also to Mars and others will make research in this setting available to pursue at universities worldwide. In this context, our aim is to provide a first approach to deal with the data collected by NASA Perseverance and extract purposeful

information. We first visualize the data, for instance by the use of K-means Clustering and t-SNE (t-distributed Stochastic Neighbor Embedding), and then extract a subset of the samples useful for the application under consideration. In our case we focus on synthetic image generation and instance segmentation and then finally go through thorough testing, analysis and review of the algorithms used and the results obtained.

2 Overview

With the advent of Deep Learning, applications that rely on huge amounts of data have emerged to be game changers in a wide range of topics and across the disciplines. The dramatic improvement in accuracy and speed has paved the way for the first time to use automated learning techniques in scenarios where reliability is key, such as safety-critical systems and self-driving cars. The use of these techniques in space exploration is starting to take place; as conditions in other planets are adverse for humans, robots are in charge of teleoperated missions on their own prior to human settlement. Autonomy will be crucial for the possibility of humanity to establish elsewhere.

In this work we initiate a journey through several techniques that will give us the ability to understand the data, analyse it and even generate new synthetic samples, sometimes indistinguishable at the human eye by learning the original distribution by the use of examples and sampling from it. We will also extract semantic information from the collected images as a way to show that we can apply successfully on other planets the same techniques we use on Earth for systems that learn by itself. These algorithms are the seed for more complex enterprises under the condition of scarce data. After all, our ability to compile large amounts of information from other planets is bounded, such as SLAM and VIO.

3 Data Collection

The first stage of our study consists on data collection. We provide scripts to massively scrape data from NASA Website³ using the tools Selenium⁴ and BeautifulSoup⁵. Images from NASA Perseverance and Curiosity are provided in the project webpage. Scripts and detailed information of the process of data acquisition can be found in our repository on GitHub⁶.

³ <https://mars.nasa.gov/>

⁴ <https://www.selenium.dev/>

⁵ <https://www.crummy.com/software/BeautifulSoup/>

⁶ <https://github.com/decurtoidiaz/cyz>

4 Visualization

With the aim of using a subset of the collected data for synthetic image generation and instance segmentation, we visualize the data to look for a significant portion of the samples to use, and identify outliers and points outside the distribution. Also, it is important to consider that images are taken using contrasting configurations of cameras; and we choose a subset that describes well the terrain of the surface of Mars. The techniques under study are K-means Clustering with a prior projection on the 2D plane by the use of PCA(2) and t-SNE with a prior reduction of dimensionality using PCA which adjusts the number of Principal Components to explain for 99% of variance, Figure 1.

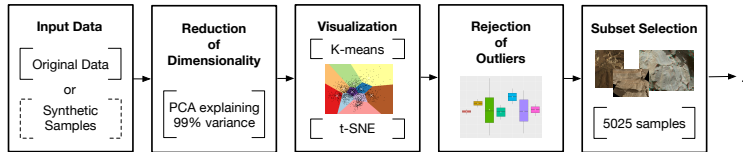


Fig. 1: Visualization pipeline under study.

4.1 K-means Clustering

We project the data into a 2D plane by the use of PCA and then apply K-means Clustering, where k is the number of cameras used on each mission. Due to the high dimensionality of the problem, the need to use a more sophisticated technique arises. The resultant projection does not show well defined clusters and not all outliers are correctly rejected. K-means Clustering is a lineal technique and a lot of information is lost on the 2D plane projection. So we then propose to use t-SNE which is based on a probabilistic measure to accomplish the task. We introduce an adaptive t-SNE technique with a varying degree of explainability of variance given by PCA.

4.2 t-SNE

t-SNE (t-Distributed Stochastic Neighbor Embedding) was proposed in [41] and introduces a probabilistic technique to visualize and understand high-dimensional data such as images. We perform a prior dimensionality reduction by the use of PCA, in which we choose adaptively the number of Principal Components that explains the 99% of the variance, Figure 2. Proposing then a PCA adaptive t-SNE. Having this adaptive behavior is central to the task at hand to extend the validity of the technique to a varying number of data points, camera settings, and changing environments.



Fig. 2: K-means Clustering (left) and t-SNE (right) on images from NASA Curiosity (upper figures) and Perseverance (lower figures).

This technique allows us to select a subset of the original data taken by MastCam-Z which is useful for synthetic terrain generation and instance segmentation. It helps identify out-of-distribution points, and clusters together all images pertaining to cameras pointing to martian terrain. The subset of data is released as a dataset on its own⁷, both in PNG image format and in TFRecords for rapid importation and training.

5 Synthetic Generation of Samples

The field of synthetic image generation has seen rapid progress. The necessity to generate synthetic imagery given some training data in many applications (simulated environments, additional training data, style-transfer) has seen great research efforts to establish a stable, principled way to accomplish the task. Generative Adversarial Networks (GANs) [13,36,1,38,32,33,18,23,22] and VAE (Variational AutoEncoders) [25] offer stable training mechanisms to achieve convergence. Yet, more progress is needed as the capacity of the network is mainly bounded by the GPU memory and training resources available [7,10,46,20,43,3]. Results often suffer from mode collapse and gradient explosion, and its good performance to accomplish complex tasks such as generating additional multi-view frames is yet to be proven.

The work presented in [39] introduced a new type of generative model based on annealed Langevin [37,44]. The method is further developed in [40], where they show competitive image generation. Diffusion Probabilistic Models [17] achieved state-of-the-art results on CIFAR10 building on the same principles derived from diffusion-based methods [14]. However, Score-based Generative Models [19] suffer from the same drawbacks of GANs and their real-time implementation is not viable due to the sampling step where the dimension of the output must be the same as the dimension of the input. That is, they are hugely dependent on GPU memory resources and necessitate high computing time.

Supplemental recent approaches [47] are based on the attention mechanism [42] building mainly on Vision Transformers [11]. Other techniques like NeRF

⁷ <https://github.com/decurtoidiaz/drcyz>

[34] could be essential to add structure to the learning paradigm. In the context of space exploration, these techniques could have a huge impact, as the number of data is by definition scarce; although diminishing, due to our limitation to collect high-resolution data in other planets. Bandwidth and latency of operating a commercial robot at thousands of km from Earth severely limit the real-time data acquisition and capacity of reaction of human-controlled rovers. Indeed, being able to synthesize new useful data from few observations could enable fast and improved SLAM and VIO, as well as enhance autonomous capabilities of the extraterrestrial robot counterparts. We focus on the problem of generating synthetic images with a limited amount of data, being Stylegan2-ADA [21] the baseline method of choice for our studies.

5.1 Stylegan2-ADA

GANs learn a probability distribution from samples by training concomitantly two networks, and the Generator (G) produces images that resemble the original training instances while the Discriminator (D) determines their fidelity. The networks are trained until convergence in a zero-sum game fashion. Reference [21] goes beyond the common GAN architecture by leveraging the concept of Stochastic Discriminator Augmentation and proposing an Adaptive Discriminator Augmentation (ADA) that helps the network converge to same accuracy levels as before but with a few thousand samples; which makes it ideal for our application. We train the network with a subset of 5025 samples from the NASA Perseverance mission using an NVIDIA-P100 on the cloud during 48h. The results obtained are consistent. We sample the trained model to generate 100, 1000 and 10000 samples, see Figure 3; and release the data publicly for testing purposes.

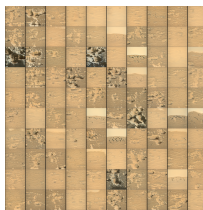


Fig. 3: Grid of 100 samples generated by Stylegan2-ADA trained at size 256x256 using samples from NASA Perseverance.

5.2 Score-based Generative Modeling

Based on annealed langevin [39,40], Score-based Generative Modeling introduces a new way to generate synthetic data as an alternative to adversarial learning

in GANs.

We conduct synthetic image generation using grayscale data from NASA Perseverance at image size 28×28 and sample the learned distribution using PC (Predict-Correct) Sampling, Euler-Maruyama, and ODE Sampling, Figure 4.

If we then compute the likelihood on the dataset by the use of the learned model and a batch size of 32 we get an average number of bits per dimension of 6.18. In comparison for example to an average number of bits per dimension on MNIST of 3.98. This means the subset of samples from NASA Perseverance we have chosen is a good candidate to test learning models such as GANs and Score-based Generative Modeling because the learned latent spaces have to incorporate complex features such as description of the terrain, rocks and sky while keeping the number of samples low.

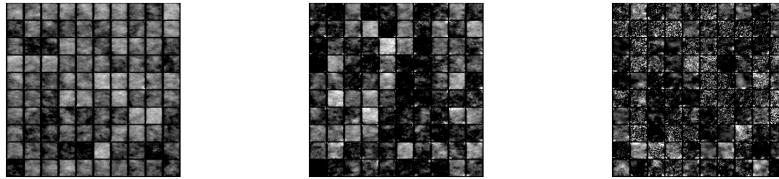


Fig. 4: Grid of 100 samples generated by PC Sampling (left), Euler-Maruyama (middle) and ODE Sampling (right). The models are trained at size 28×28 during 71 epochs using samples from NASA Perseverance.

6 Statistical Analysis of the Generated Distribution

Considering the original subset of data from NASA Perseverance and the generated synthetic dataset of 1000 images as two distributions we want to compare, we propose a preliminary statistical analysis by means of a non-parametric test: Kruskal-Wallis [27]. In order to proceed with the evaluation, we compute the mean of the RGB image intensities or gray-scale as a proxy of image descriptor; although unadorned, mean intensity can provide rough texture information for an initial assessment. We first test the homoscedasticity, or equality of variances, by means of the test of Levene; and we also test for normality of the two distributions. Finally we compute goodness of fit by Kruskal-Wallis. In the case of homoscedasticity we reject the null hypothesis (significant p -value less than 0.05), same for normality of the original distribution (as expected as the original samples do not follow a Gaussian distribution). In the case of the synthetic samples, we accept the null hypothesis for the case of normality and we can assure the distribution is normal, which makes sense as the GAN architecture models initially the samples as noise White Gaussian and then modifies them step by

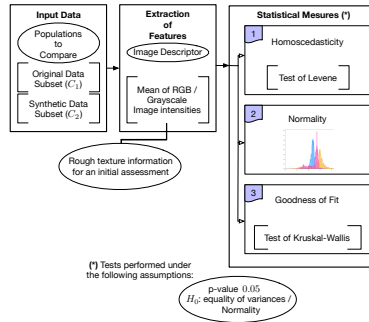


Fig. 5: Statistical measures to study goodness of fit to initially assess GAN convergence.

step to fit the original distribution. We cannot accept though the null hypothesis for goodness of fit, which means that a more sophisticated way of measuring the sample quality in GAN has to be proposed, as has already been extensively seen in the current literature. For example, MS-SSIM [36] and FID [16] are the most accepted measures. However, this simple non-parametric analysis, Figure 5, can serve as a unit test for GAN and other variational methods once the model is trained and the authors have not seen it widely used in the community so far.

Table 1: Interpretation of statistical measures given the proposed pipeline under study, Figure 5.

Test	Population	Result	Interpretation
1	C_1 and C_2	✓	(a)
		✗	(b)
2	C_2	✓	(c)
		✗	(d)
3	C_1 and C_2	✓	(e)
		✗	(f)

Description and interpretation of statistical measures in Table 1.

- (a) Necessary condition but not sufficient to assert that both populations originate from the same distribution.
- (b) There is not enough statistical evidence to attest both populations samples originate from the same distribution.
- (c) With high probability the synthetic distribution generated is still close enough to the initial distribution of noise from the GAN architecture. The samples may not show enough fidelity, and there is probably bad generalization behavior.

- (d) The synthetic distribution is far from the initial distribution of noise and has deviated from the original Normal and may be close to the target distribution.
- (e) If (a) then there is enough statistical evidence to confirm that both populations originate from the same distribution given this image descriptor.
- (f) There is not enough statistical evidence to attest both populations are from the same distribution.

We have proposed statistical measures and a visualization pipeline to study and understand the data under consideration. However, the highly dimensional nature of images and the fact that video streams are sequential introduces a notion of time and space that our analysis has not taken into consideration. Indeed, the data consists on a sequence of images captured during a given lineal period of time following a specific path on the surface of Mars. To this effect, in the next section we borrow tools from harmonic analysis to provide further interpretation.

7 Signature Transform and Harmonic Analysis

The Signature Transform [2,24,8,28,35] is a roughly equivalent to Fourier; instead of extracting information about frequency extracts information about order and area.

Howbeit, the Signature Transform differs from Fourier by the fact that it utilizes a basis of the space of functions of paths, a more general case to the basis of space of paths found in the preceding.

Following [2], the truncated signature of order N of the path \mathbf{x} is defined as a collection of coordinate iterated integrals

$$S^N(\mathbf{x}) = \left(\left(\int_{0 < t_1 < \dots < t_a < 1} \prod_{c=1}^a \frac{df_{z_c}}{dt}(t_c) dt_1 \dots dt_a \right)_{1 \leq z_1, \dots, z_a \leq d} \right)_{1 \leq a \leq N} . \quad (1)$$

The Signature is a homomorphism from the monoid of paths into the group-like elements of a closed tensor algebra, Equation 2. It provides a graduated summary of the path \mathbf{x} . These extracted features of a path are at the center of the definition of a rough path [30]; they remove the necessity to take into account the inner detailed structure of the path.

$$S : \{f \in F \mid f : [x, y] \rightarrow E = \mathbb{R}^d\} \longrightarrow T(E) = T(\mathbb{R}^d) = \prod_{c=0}^{\infty} (\mathbb{R}^d)^{\otimes c} . \quad (2)$$

It has many advantages over other tools of harmonic analysis for ML. It is a universal non-linearity, which means that every continuous function of the input

stream may be approximated arbitrary well by a linear function of its signature. Also, among other properties, presents outstanding robustness behavior to missing or irregularly sampled data along with optional invariance in terms of translation and sampling. It has recently been introduced in the context of Deep Learning to add some structure to the learning process; and seems a promising tool in Generative Models and Reinforcement Learning; as well as a good theoretical framework. It mainly works on streams of data which could describe from video sequences to all the set of our life experiences. Scilicet, under the correct assumptions and the right application, it could potentially compress all human experiences in a representation that could be stored and processed efficiently. Here we propose to do a preliminary study in terms of harmonic analysis and understand its properties to compare the original and synthetic samples.

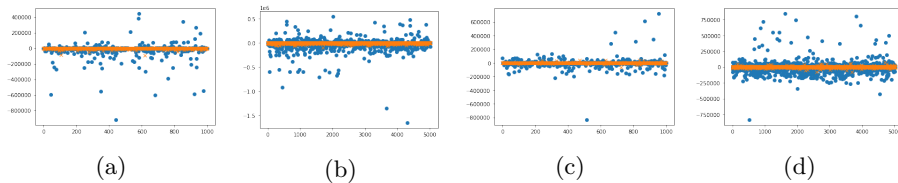


Fig. 6: Spectrum of the mean signature (a,b) and log-signature (c,d) of a 64-dimensional path up to level 3 of original ('o') against 1000 (a,c) and 5000 (b,d) synthetic ('x') samples.

The Signature [30,26,15,4,12] of an input stream of data encodes the order in which data arrives without caring precisely when it arrives. This property which is known as invariance to time reparameterisations [29], makes it an ideal candidate to measure GAN generated distributions against an original data stream. That is to say, when sampling the GAN model, instances of the latent space are retrieved in no specific order although the original data is by definition time dependent, as recorded video streams or image captured by sensors are constrained and bounded by time physics. However, GANs are not able to generate yet data lineally in time and space, and thus the comparison using other methods may be biased or not take into account all the relevant cues.

Withal, it is important to note that the number of components of the truncated signature does not depend on the number of data samples into consideration. Namely, it maps the infinite-dimensional space of streams of data $\mathcal{S}(\mathbb{R}^d)$ into a finite-dimensional space of dimension $(d^{N+1} - 1)/(d - 1)$, where N corresponds to the order of the truncated signature, which makes it very appropriate to process long sequential data with varying length or unevenly sampled data.

At the same time, we can introduce the concept of log-signature [28,35], which is a more compact representation than the Signature.

Definition 1. If $\gamma_t \in E$ is a path segment and S is its Signature then

$$\begin{aligned} S &= 1 + S^1 + S^2 + \dots \quad \forall c, S^c \in E^{\otimes c} \\ \log(1+x) &= x - x^2/2 + \dots \\ \log S &= (S^1 + S^2 + \dots) - (S^1 + S^2 + \dots)^2/2 + \dots \end{aligned}$$

The series $\log S = (S^1 + S^2 + \dots) - (S^1 + S^2 + \dots)^2/2 + \dots$ which is well defined, is referred to as the log-signature of γ .

Unlike the Signature, the log-signature does not guarantee universality [30] and thus it needs to be combined with non-linear models for learning. However, it is empirically more robust to sparsely sampled data. There is a one-to-one correspondence between the Signature and the log-signature as the logarithm map is bijective [31,28]. This statement also holds true for the truncated case up to the same degree.

In this line of work, we perform a comparison of the mean signature and log-signature of original against synthetic samples at size 64×64 and observe that synthetic samples encompass the most relevant information from the original harmonic distribution, see Figure 6. We compare against a set of 1000 and 5000 synthetic samples and each instance is considered to be a path \mathbf{x} of dimension 64 to which we apply the Signature and log-signature transforms.

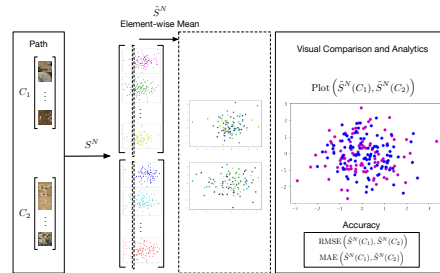


Fig. 7: Visual explanation of the use of \tilde{S}^N to analyze GAN convergence. Samples are resized at 64×64 and transformed to grayscale previous to the computation of the signatures. The procedure used for log-signature $\log \tilde{S}^N$ is analogous.

7.1 RMSE and MAE Signature and Log-signature

We propose to use the element-wise mean of the truncated signatures \tilde{S}^N , Figure 7, to analyse the convergence of GAN learned models by the use of RMSE (Root Mean Squared Error) and MAE (Mean Absolute Error); we name the measures RMSE and MAE Signature and RMSE and MAE log-signature. For instance, in



Fig. 8: Spectrum of the element-wise mean of the signatures (left) and log-signatures (right) of order 3 and size 64×64 of original ('o') against synthetic ('x') samples.

Figure 8 we can observe that the model is attaining good convergence, although is not capturing all the information present in the original distribution.

RMSE and MAE Signature and log-signature can be used not only to compare models but also to keep performance of training across several epochs and analytically detect overfitting, Table 2. Although all measures capture information about the visual cues present in the distributions, RMSE and MAE Signature and MAE log-signature are more accurate at keeping track of the GAN training procedure convergence, while RMSE log-signature is less precise.

Table 2: RMSE and MAE Signature and log-signature across several iterations of training of Stylegan2-ada (lower is better). Our synthetic samples are generated using the model 798 which achieves the highest RMSE and MAE Signature and MAE log-signature accuracy.

Iteration Stylegan2-ada	193	371	596	798	983
RMSE Signature	15617	13336	12353	11601	25699
MAE Signature	11072	10686	9801	9086	19481
RMSE log-signature	9882	7563	7354	7397	15621
MAE log-signature	6467	5955	5724	5717	12063

7.2 Evaluation

We enclose results of the proposed measures using several state-of-the-art pretrained models, Table 3. For the evaluation and testing we use the standard AFHQ dataset [9] classes 'cat', 'dog' and 'wild' and MetFaces [21], together with the corresponding pretrained models. To compute RMSE and MAE \tilde{S}^N and $\log \tilde{S}^N$ we generate 1000 synthetic samples of each model and compare against the full original dataset. The samples are transformed to grayscale and resized at 64×64 previous to the Signature Transform. Visual comparison of the spectrum is provided in Figures 9 and 10 where it can be seen that the trained models are actually learning the empirical distribution of the original data.

In Table 3 we compare the recently developed models $\{r, t\}$ -Stylegan3-ada [22] against Stylegan2-ada using MetFaces, where we can see that t -Stylegan3-

ada clearly outperforms Stylegan2-ada and r -Stylegan3-ada, which agree with the FID results reported in [22]. Visual comparison of the spectrum of the Signatures for the given dataset can be seen in Figure 10.

Table 3: RMSE and MAE Signature and log-signature evaluation and comparison on AFHQ and MetFaces using state-of-the-art pretrained models of Stylegan2-ada [21] and Stylegan3-ada [22].

Model	Dataset	RMSE \tilde{S}^3	MAE \tilde{S}^3	RMSE $\log \tilde{S}^3$	MAE $\log \tilde{S}^3$
Stylegan2-ada	Cat	61450	45968	29201	22297
	Dog	38861	30441	31686	24612
	Wild	33306	25578	26622	20359
r -Stylegan3-ada	MetFaces	33247	23428	25685	18071
t -Stylegan3-ada		30894	19872	21560	13761

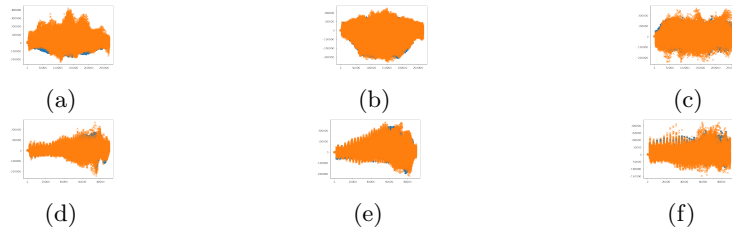


Fig. 9: Spectrum of the element-wise mean of the signatures \tilde{S}^3 (top) and log-signatures $\log \tilde{S}^3$ (bottom) of order 3 and size 64×64 of original ('o') against synthetic ('x') samples. (a,d): AFHQcat, (b,e): AFHQdog, (c,f): AFHQwild.

8 Instance Segmentation

Instance Segmentation is the problem of assigning to each pixel a corresponding semantic label according to some training attributes of choice. This formulation can be of utmost importance in many applications, from self-driving vehicles to drone guidance in unknown environments (e.g. the NASA helicopter Ingenuity). The extraction of semantic information from visual sensors is one of the enablers of intelligence as we humans conceive it. After all, visual input is our main source of trigger towards actionable tasks; and man-made robots as we have conceived them do suffer or are blessed from this fact. However, current trend in robotics allows to fuse this information with input from other sensors, such as LiDARs, radars, event-cameras, low-power bluetooth (UWB) [45] and even audio features.

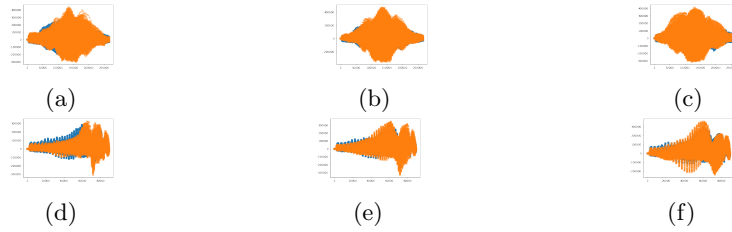


Fig. 10: Spectrum comparison of the element-wise mean of the signatures \tilde{S}^3 (top) and log-signatures $\log \tilde{S}^3$ (bottom) of order 3 and size 64×64 of original ('o') against synthetic ('x') samples from MetFaces. (a,d): Stylegan2-ada, (b,e): *r*-Stylegan3-ada, (c,f): *t*-Stylegan3-ada.

We will focus here though mainly on the study of visual information, and let for future works the mixture of other sensor inputs.

We propose an initial pipeline for instance segmentation on the surface of Mars by using a model DeepLab-v3 [6,5] pre-trained on the dataset ADE20K [48], which contains many samples from terrains on Earth with attributes that can appear on Mars (rocks, sky, sand, terrain). We use the model without re-training or finetuning, Figure 11, as we do not possess segmentation masks of the given samples.

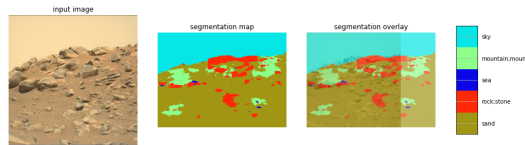


Fig. 11: Segmentation of a given sample without re-training on samples from Mars using Deeplab-v3 trained on ADE20K.

Finetuning on a subset of the samples from Mars, e.g. 200 correctly labeled instances, would allow for state-of-the-art results on real-time data sent by a rover acting as a relay on the surface of the planet.

9 Other Applications

Beyond synthetic image generation and instance segmentation, which are indeed intermediate steps for other tasks, the main goal of using automated learning techniques in space exploration is the capacity to provide robots with a high-degree of autonomy so that they can explore efficiently the surface of other

planets. Teleoperation is hard in a context where bandwidth and latency depend on many factors, and the higher the autonomy we confer to the rovers, the greater will be the benefits of a continued presence of humanity in other celestial bodies. As a consequence, one application in this regard that is capital is the ability to model 3D environments as accurately as possible⁸. Being style-transfer from simulation, see Figure 12, to super-realistic images one of the main utilizations of GANs and synthetic image generation in this context. Furthermore, having accurate positioning measurements to contrast against other sensor inputs is very important when dealing with self-driving vehicles. And therefore, being able to process visual imagery while extracting telling information, such as visual cues to understand and predict future trajectories, discovering possible paths to avoid obstacles, having accurate recognition of elements in the environment, and real-time weather and temperature forecast of varying paths to plan precisely for any inconvenient without the need of human intervention. They are among the most pressing applications that need immediate attention from the research community.



Fig. 12: NASA Curiosity simulator that lets you explore the surface of Mars.

10 Conclusions

In this paper, we have presented a pipeline for visual understanding of the imagery captured by the sensors of robots in other planets to introduce an adaptive technique based on t-SNE and PCA that without the need of hyperparameter tuning puts forward exceptional visualization capabilities of the missions. We compare the technique against traditional K-means Clustering to see its many advantages. Furthermore, we go beyond and generate synthetic samples from the surface of Mars by the use of Stylegan2-ADA and propose an effective methodology to statistically test their goodness-of-fit according to the original distribution. Additionally, we conduct synthetic image generation by the use of Score-based Generative Modeling and experiment with several methods of sampling. We are also the first to propose the use of the Signature Transform to assess GAN convergence by introducing RMSE and MAE Signature and log-signature. Semantic understanding of the samples is achieved through state-of-the-art instance segmentation and we gain insights on how superior performance in other planets could be attained by leveraging networks trained on data from Earth.

⁸ <https://eyes.nasa.gov/curiosity/>

Acknowledgements

This work is supported by HK Innovation and Technology Commission (InnoHK Project CIMDA) and HK Research Grants Council (Project CityU 11204821).

References

1. Antoniou, A., Storkey, A., Edwards, H.: Data augmentation generative adversarial networks. ICLR (2018)
2. Bonnier, P., Kidger, P., Arribas, I.P., Salvi, C., Lyons, T.: Deep signature transforms. NIPS (2019)
3. Brock, A., Donahue, J., Simonyan, K.: Large scale gan training for high fidelity natural image synthesis. ICLR (2019)
4. Chang, J., Lyons, T.: Insertion algorithm for inverting the signature of a path. arXiv:1907.08423 (2019)
5. Chen, L., Papandreou, G., Schroff, F., Adam, H.: Rethinking atrous convolution for semantic image segmentation. arXiv:1706.05587 (2017)
6. Chen, L., Papandreou, G., Kokkinos, I., Murphy, K., Yuille, A.L.: DeepLab: Semantic Image Segmentation with Deep Convolutional Nets, Atrous Convolution, and Fully Connected CRFs. TPAMI (2017)
7. Chen, Q., Koltun, V.: Photographic image synthesis with cascaded refinement networks. IEEE International Conference on Computer Vision (2017)
8. Chevyrev, I., Kormilitzin, A.: A primer on the signature method in machine learning (2016)
9. Choi, Y., Uh, Y., Yoo, J., Ha, J.: Stargan v2: Diverse image synthesis for multiple domains. CVPR (2020)
10. Dosovitskiy, A., Brox, T.: Generating images with perceptual similarity metrics based on deep networks. NIPS (2016)
11. Dosovitskiy, A., Beyer, L., Kolesnikov, A., Weissenborn, D., Zhai, X., Unterthiner, T., Dehghani, M., Minderer, M., Heigold, G., Gelly, S., Uszkoreit, J., Houlsby, N.: An image is worth 16x16 words: Transformers for image recognition at scale. ICLR (2020)
12. Fermanian, A.: Learning time-dependent data with the signature transform. Theses, Sorbonne Université (2021), <https://tel.archives-ouvertes.fr/tel-03507274>
13. Goodfellow, I., Pouget-Abadie, J., Mirza, M., Xu, B., Warde-Farley, D., Ozair, S., Courville, A., Bengio, Y.: Generative adversarial networks. NIPS **27** (2014)
14. Goyal, A., Ke, N.R., Ganguli, S., Bengio, Y.: Variational walkback: Learning a transition operator as a stochastic recurrent net. NIPS (2017)
15. Graham, B.: Sparse arrays of signatures for online character recognition (2013)
16. Heusel, M., Ramsauer, H., Unterthiner, T., Nessler, B., Hochreiter, S.: GANs trained by a two time-scale update rule converge to a local nash equilibrium. NIPS **30** (2017)
17. Ho, J., Jain, A., Abbeel, P.: Denoising diffusion probabilistic models. NIPS (2020)
18. Jolicoeur-Martineau, A.: The relativistic discriminator: a key element missing from standard GAN. ICLR (2019)
19. Jolicoeur-Martineau, A., Piché-Taillefer, R., des Combes, R.T., Mitliagkas, I.: Adversarial score matching and improved sampling for image generation. ICLR (2021)

20. Karras, T., Aila, T., Laine, S., Lehtinen, J.: Progressive growing of GANs for improved quality, stability, and variation. ICLR (2018)
21. Karras, T., Aittala, M., Hellsten, J., Laine, S., Lehtinen, J., Aila, T.: Training generative adversarial networks with limited data. NIPS (2020)
22. Karras, T., Aittala, M., Laine, S., Härkönen, E., Hellsten, J., Lehtinen, J., Aila, T.: Alias-free generative adversarial networks. NIPS (2021)
23. Karras, T., Laine, S., Aila, T.: A style-based generator architecture for generative adversarial networks. CVPR (2019)
24. Kidger, P., Lyons, T.: Signatory: differentiable computations of the signature and logsignature transforms, on both CPU and GPU. ICLR (2021)
25. Kingma, D.P., Welling, M.: Auto-encoding variational bayes. ICLR (2014)
26. Kiraly, F.J., Oberhauser, H.: Kernels for sequentially ordered data. JMLR **20**(31), 1–45 (2019)
27. Kruskal, W.H., Wallis, W.A.: Use of ranks in one-criterion variance analysis. *Journal of the American Statistical Association* **47**(260), 583–621 (1952). <https://doi.org/10.1080/01621459.1952.10483441>
28. Liao, S., Lyons, T.J., Yang, W., Ni, H.: Learning stochastic differential equations using RNN with log signature features. arXiv:1908.08286 (2019)
29. Lyons, T.: Differential equations driven by rough signals. *Revista Matemática Iberoamericana* **14**(2), 215–310 (1998)
30. Lyons, T.: Rough paths, signatures and the modelling of functions on streams. *Proceedings of the International Congress of Mathematicians* (2014)
31. Lyons, T., Caruana, M., Lévy, T., d’été de probabilités de Saint-Flour, É.: Differential equations driven by rough paths. Springer (2007)
32. Mescheder, L., Nowozin, S., Geiger, A.: The numerics of GANs. NIPS (2017)
33. Mescheder, L., Nowozin, S., Geiger, A.: Which training methods for GANs do actually converge? ICML (2018)
34. Mildenhall, B., Srinivasan, P.P., Tancik, M., Barron, J.T., Ramamoorthi, R., Ng, R.: NeRF: Representing scenes as neural radiance fields for view synthesis. ECCV (2020)
35. Morrill, J., Kidger, P., Salvi, C., Foster, J., Lyons, T.J.: Neural CDEs for long time series via the log-ode method. ICML (2021)
36. Odena, A., Olah, C., Shlens, J.: Conditional image synthesis with auxiliary classifier gans. ICML (2017)
37. Roberts, G.O., Tweedie, R.L.: Exponential convergence of Langevin distributions and their discrete approximations. *Bernoulli* **2**(4), 341 – 363 (1996)
38. Salimans, T., Goodfellow, I., Zaremba, W., Cheung, V., Radford, A., Chen, X.: Improved techniques for training GANs. NIPS (2016)
39. Song, Y., Ermon, S.: Generative modeling by estimating gradients of the data distribution. NIPS (2019)
40. Song, Y., Ermon, S.: Improved techniques for training score-based generative models. NIPS (2020)
41. van der Maaten, L., Hinton, G.: Visualizing data using t-SNE. JMLR **9**(86), 2579–2605 (2008)
42. Vaswani, A., Shazeer, N., Parmar, N., Uszkoreit, J., Jones, L., Gomez, A.N., Kaiser, L., Polosukhin, I.: Attention is all you need. NIPS (2017)
43. Wei, X., Gong, B., Liu, Z., Lu, W., Wang, L.: Improving the improved training of wasserstein gans: a consistency term and its dual effect. ICLR (2018)
44. Welling, M., Teh, Y.W.: Bayesian learning via stochastic gradient langevin dynamics. ICML (2011)

45. Xu, H., Wang, L., Zhang, Y., Qiu, K., Shen, S.: Decentralized visual-inertial-UWB Fusion for relative state estimation of aerial swarm. ICRA (2020)
46. Zhao, J., Mathieu, M., LeCun, Y.: Energy-based generative adversarial networks. ICLR (2017)
47. Zhao, L., Zhang, Z., Chen, T., Metaxas, D.N., Zhang, H.: Improved transformer for high-resolution gans. NIPS (2021)
48. Zhou, B., Zhao, H., Puig, X., Xiao, T., Fidler, S., Barriuso, A., Torralba, A.: Semantic understanding of scenes through the ADE20K dataset. IJCV (2018)